AAS 16-258

DEEP SPACE ATOMIC CLOCK TECHNOLOGY DEMONSTRATION MISSION ONBOARD NAVIGATION ANALOG EXPERIMENT

Jill Seubert[*], **Todd Ely**[†]

The timing and frequency stability provided by the Deep Space Atomic Clock (DSAC) is on par with the Deep Space Network's ground clocks, and will enable one-way radiometric measurements with accuracy equivalent to current two-way tracking data. A demonstration unit of the clock will be launched into low Earth orbit in late 2016/early 2017 for the purpose of validating DSAC's performance in the space environment. GPS data collected throughout the mission will be utilized not only for precise clock estimation, but also as a proxy for deep space tracking data. Through careful processing of GPS Doppler data and limited modeling fidelity representative of onboard capabilities, onboard orbit solutions can be compared to higher-fidelity ground solutions, demonstrating DSAC's viability as an onboard navigation instrument in conditions typical for a low altitude Mars orbiter.

INTRODUCTION

The practicality of deep space navigation based solely on one-way radiometric tracking data is currently limited by the performance of the onboard clock. Compared to the very high stability and accuracy of ground atomic clocks (the National Institute of Standards and Technology's Ytterbium lattice atomic clock exhibits white frequency errors with a one-day Allan Deviation $<$ 1e-17), the performance of space-flown clocks has been lacking.[1] Ultra Stable Oscillators (USOs) exhibit long-term frequency drift that is highly correlated with the orbital parameters, and recovering large clock bias and drift terms following long periods without tracking yields significant degradations in orbit solution quality. The Deep Space Atomic Clock (DSAC) project is a NASA Technology Demonstration Mission (TDM) that will bridge the gap between ground and space clocks by validating the on-orbit performance of a small, low-mass mercury ion ($^{199}Hg^{+}$) atomic clock. Pre-flight ground testing has shown that DSAC's stability is better than 3e-15 at one day. In contrast to a USO's frequency drift, DSAC's frequency stability improves over long integration times, providing long-term stability and accuracy on par with the ground clocks in use at the Deep Space Network (DSN).

Such a small spacecraft clock error will enable one-way radiometric tracking data with accuracy equivalent to current two-way tracking data, allowing a shift to a more efficient and flexible one-way deep space navigation architecture. One such navigation architecture is the opportunity to perform

[*]Investigation System Engineer, Deep Space Atomic Clock Technology Demonstration Mission, Jet Propulsion Laboratory, California Institute of Technology, MS 301-141C, 4800 Oak Grove Drive, Pasadena, CA 91109-8099; Jill.Tombasco@jpl.nasa.gov, 818-354-4076.

[†]Principal Investigator, Deep Space Atomic Clock Technology Demonstration Mission, Jet Propulsion Laboratory, California Institute of Technology, MS 301-121, 4800 Oak Grove Drive, Pasadena, CA 91109-8099; Todd.A.Ely@jpl.nasa.gov, 818-393-1744.

©2016 California Institute of Technology. Government sponsorship acknowledged.

onboard navigation using an uplinked signal transmitted by the DSN. As discussed in Reference 2, the transition from ground-based to onboard navigation has numerous challenges driven primarily by limited computational efficiency, thus restricting onboard orbital and environmental modeling capabilities. While the high-fidelity orbit solutions produced via ground-based processing may not be possible, these solutions may also not be required for all deep space missions.

The DSAC mission will be a hosted payload onboard a Surrey Satellite Technology (SST-US) Orbital Test Bed (OTB) spacecraft, currently planned for launch into low Earth orbit (LEO) in late 2016/early 2017. Once in LEO, DSAC's space-based performance will be characterized via a yearlong demonstration, during which Global Positioning System (GPS) tracking data will be processed to produce precise orbit and clock solutions. If DSAC performs at its anticipated level, then its utility for one-way radiometric deep-space navigation can be validated by showing that orbit determination performance using the one-way data performs as well as or better than its traditional two-way counterpart. To this end, a planned deep space navigation analog experiment will utilize the GPS tracking data to demonstrate orbit determination performance using one-way and pseudo two-way GPS Doppler data with measurement quality, quantity, and schedule characteristics (such as tracking data gaps) that are operationally similar to that which is typically available in deep space navigation.

For one such navigation analog experiment, GPS data will be down-selected and the filter designed to replicate trajectory reconstruction of a low-altitude Mars orbiter. Simulation results have demonstrated that, when using high-fidelity models and filter configurations typical to ground-based navigation operations, the OTB orbit can be reconstructed to a formal uncertainty of less than 1 meter (3σ) during tracking passes and is inflated by $\approx$ 25 cm during lengthy tracking gaps.[3] As discussed in Reference 2, high-fidelity dynamic models and advanced filtering techniques may not be feasible for onboard computing; by limiting the model fidelity and filter configuration when processing the flight GPS data, the nominal experiment will be extended to simulate onboard navigation of a low-altitude Mars orbiter. This work assesses candidate dynamic modeling and filter simplifications and their impact on filter performance, as measured both by orbit determination accuracy and processing time.

DSAC TECHNOLOGY DEMONSTRATION MISSION

The DSAC TDM will verify the clock's space performance and demonstrate the viability of $^{199}Hg^{+}$ atomic space clock technology for navigation purposes. DSAC technology uses the stability of the mercury ions' hyperfine transition frequency at 40.5 GHz to effectively steer the frequency output of a quartz crystal USO to a near-constant value.[4] The mercury ions are confined in a trap with applied electric fields and protected from perturbations via applied magnetic fields and shielding. This provides a stable environment for measuring the hyperfine transition very accurately and minimizes sensitivity to temperature and magnetic variations that will be encountered on orbit. Given this enhanced clock stability and the fact that the system has almost no expendables, the DSAC clock technology is suitable for very long-duration space missions. Following a successful yearlong TDM, the clock technology will be advanced from a Technology Readiness Level (TRL) 5 to TRL 7.

The SST-US OTB spacecraft will be launched into a near-circular, near-equatorial orbit by a Space Exploration Technologys (SpaceX) Falcon Heavy rocket, as a secondary payload of the United States Air Force Space Technology Program II. The nominal deployed OTB spacecraft configuration and orbital orientation are shown in Figure 1. The spacecraft mass is $\approx$ 180 kg, has no

active propulsion system and is nominally oriented with the solar arrays pointed in the zenith direction. The current best estimate (as of January 2016) of DSAC's size, weight, and average power are 29 cm x 26 cm x 23 cm, 16.5 kg, and 46.6 W, respectively. Figure 2 shows a computer model of DSAC on the left and the assembled flight hardware on the right (mounted to baseplate). In addition to the atomic clock demonstration unit, the DSAC payload also includes an oversized crystal USO and a GPS system comprised of a JPL-designed TriG Precise Orbit Determination (POD) receiver and a zenith-pointing choke ring antenna (antenna shown in Figure 1).

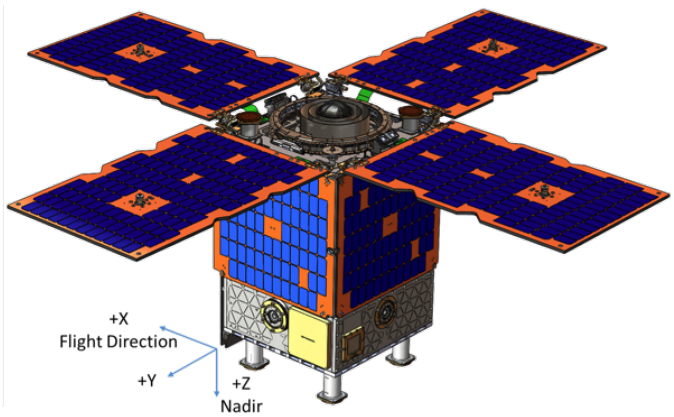

Figure 1. Nominal deployed OTB spacecraft configuration and on-orbit orientation (figure provided by SST-US).

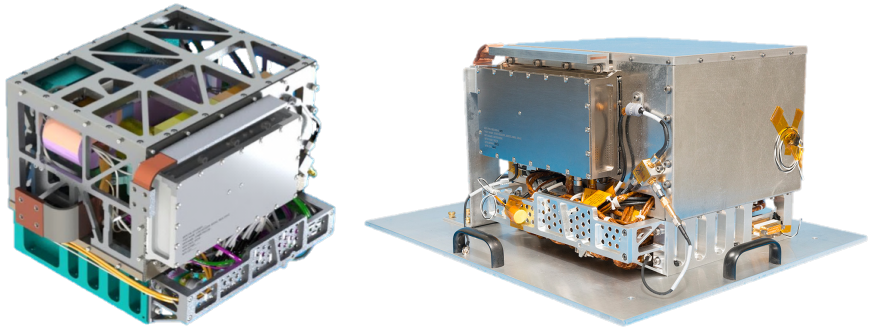

Figure 2. DSAC payload CAD model (left) and assembled flight hardware (right).

Throughout a six-month on-orbit period, the GPS subsystem will collect L1 and L2 GPS phase and pseudo-range measurements for use in satisfying the two primary objectives of the DSAC TDM: to verify the clock's stability and drift with an AD $<$ 2.0e-14 at one day while in orbit, and to demonstrate the clock's viability as a navigation tool by reconstructing the orbit to within 10 m uncertainty (3σ) in a tracking and data configuration analogous to deep space operations. The expected performance of the clock, based on pre-flight ground testing, is $<$ 3.0e-15 at one day. The requirement is looser than the expected clock performance to account for systematic errors in the measurement system; however, the performance of the validation system is expected to be better

than this required level.[3] The clock telemetry will be monitored for an additional 6 months after the active mission operations have completed to verify longer duration health and status.

OTB Orbital Environment

DSAC's performance will be evaluated in the LEO space environment, and as such evaluation of the clock performance will necessitate high-fidelity models of the orbital dynamics and GPS measurements. Additionally, the expected modeling errors that will be encountered on orbit must be characterized. Reference 3 presents detailed information regarding the nominal dynamic and measurement environment and expected errors. A brief summary is provided here.

Nominal Models The set of high-fidelity dynamic models applied during numerical integration of the OTB trajectory include the Earth Gravitational Model (EGM)-96 360x360 Earth gravitational potential,[5] Newtonian luni-solar gravity, solar radiation pressure, atmospheric drag with the Drag Temperature Model (DTM)-2012 density model, and Earth albedo and thermal emissivity pressure. The solar radiation pressure and atmospheric drag accelerations depend on a model of the OTB spacecraft; this model is comprised of 8 flat plates, representing the six-sided bus and solar array topsides and undersides, and oriented in the nominal spacecraft-fixed frame as shown in Figure 1. The diffuse and specular reflectivity properties of all major surface materials have been provided by SST-US and are included in the nominal spacecraft model.

The GPS pseudo-range and phase measurement models include the geometric range from the GPS transmit antenna to the OTB choke ring antenna, transmitter and receiver clocks, antenna locations and phase center offsets, multipath (models to be empirically constructed during the on-orbit commissioning phase), GPS receiver temperature effects, and phase wind up (GPS phase). The GPS satellite orbits and clocks are nominally defined by the Jet Propulsion Laboratory Analysis Center's publicly-available Final data products. Single-frequency (L1 and L2) data will be linearly combined to produce first-order ionosphere-free LC (phase) and PC (pseudo-range) measurements.

Expected Model Errors Current best estimates of expected on-orbit errors have been identified and are included in the high-fidelity simulations. These errors include perturbations to the nominal spacecraft attitude, DSAC clock, atmospheric density, GPS orbits and clocks, multipath model, antenna phase center location relative to center of mass, reference clock, solar pressure, GPS receiver temperature calibration, and thermal noise. Additionally, GPS receiver resets are modeled as a complete loss of data for six minutes, occurring randomly at a rate of three times per day. The error models implemented into the simulated truth trajectory and measurements are summarized in Table 1. Reference 3 contains a detailed description of each error model and its implementation. The temperature calibration models have since been updated via empirical testing; to first order, the phase and psuedo-range conversion factors are approximately -165 ps/C° and 142 ps/C°, respectively. Thermal modeling of the DSAC hardware and OTB indicates that the per-orbit temperature variations at the GPS baseplate vary on the order of 5° C peak-to-peak (P2P) around some quasi-static temperature T_0 (in the cold season this is $\approx$15° C and in the hot season $\approx$ 38° C).

DEEP SPACE ANALOG EXPERIMENT

Although DSAC will be demonstrated on a LEO platform, the on-orbit navigation experiment leverages the similarities between OTB and Mars orbiter environments and tracking geometry to validate DSAC's performance in comparable conditions. The flight experiment will (and this work does) utilize the Jet Propulsion Laboratory's Mission-analysis, Operations, and Navigation Toolkit

Table 1. Summary of Simulated Model Errors

Parameter	Error Model
OTB attitude	White noise In sunlight: $\sigma_x = \sigma_z = 0.6°$, $\sigma_y = 0.8°$ In shadow: $\sigma_x = \sigma_y = \sigma_z = 1.5°$
DSAC clock	White frequency noise AD = 3e-15 at 1 day
Atmospheric drag	ECRV $\sigma = 0.1$, $\tau = 30$ sec
GPS orbits & clocks	Final Products - Rapid Products
Multipath	GRACE-A phase map
Thermal noise	White noise LC = N[0, 1] cm PC = N[0, $\sqrt{10}$] m
Phase center location relative to center of mass	Random bias $\sigma_x = \sigma_y = \sigma_z = 5/\sqrt{3}$ mm
Reference clock	White frequency noise AD = 5e-16 at 1 day
Solar pressure	ECRV $\sigma = 0.1$, τ = 1/2 x orbital period
GPS receiver temperature	Periodic + white noise LC = -41.25 $\sin(nt + T_0)$ ps, N[0, 40] ps PC = 35.50 $\sin(nt + T_0)$ ps, N[0, 40] ps

Environment (Monte) software. Monte is a highly-capable and flexible software tool for trajectory integration, trajectory targeting, orbit determination, and statistical maneuver analysis for support of JPL flight project development and operations. Careful setup of the OTB orbit determination experiment can ensure that the LEO navigation validation is a suitable surrogate for a deep space technology demonstration of one-way radiometric navigation given DSAC's expected on-orbit performance. A detailed description of the nominal deep space analog experiment designed to satisfy the TDM requirement may be found in Reference 3; the measurement models, tracking data assumptions, and navigation filter setup are summarized here.

GPS Doppler Measurements

Deep space navigation is traditionally performed using radiometric Doppler and range tracking data. In order to serve as an analog to deep space navigation, the DSAC on-orbit navigation experiments will be conducted with "operationally similar" data types and tracking schedules. As the flight data is limited to GPS pseudo-range and phase measurements, the phase measurements are manipulated to construct GPS Doppler tracking data.

One-way GPS Doppler One-way GPS Doppler measurements, analogous to one-way DSN Doppler, may be constructed by differencing the dual-frequency GPS phase data.

$$\Delta f(t - \frac{T}{2}) = \frac{f_{LC}}{cT}(\phi_t - \phi_{t-T}) \tag{1}$$

Eq. 1 expresses the GPS Doppler measurement Δf as a function of the LC frequency f_{LC}, the speed of light c, the GPS phase measurement ϕ_t at time t, and the measurement count time T. For this work, the count time is selected to be 60 seconds.

The GPS Doppler measurements include both transmitter and receiver clock error. By applying the Final GPS clock solutions, the transmitter clock errors are reduced to a level below the phase measurement noise. In contrast, the receiver clock errors are entirely manifested in the one-way GPS Doppler. The one-way GPS Doppler is therefore directly analogous to uplink one-way DSN Doppler, in which the DSN transmitter clock error is negligible but the onboard clock error still contributes to the measurement.

Two-way GPS Doppler As GPS is a transmit-only navigation system, it is not possible to collect true two-way measurements during DSAC's on-orbit operations. Two-way Doppler data differs from one-way Doppler data in several significant ways. For two-way DSN data, transmitted and received at DSN ground antennas, the onboard clock error does not contribute to the measurement. As the two-way measurements are derived from the round-trip light time as compared to the one-way light time, the measurement sensitivity to the estimated dynamic state is scaled by a factor of 2. Finally, for frequencies such as S- and X-band where the radiometric signal noise is dominated by uncorrelated path-dependent effects, two-way measurements are a factor of $\sqrt{2}$ noisier than one-way measurements. Considering these points, one-way GPS Doppler can be manipulated such that it may serve as a surrogate for true two-way Doppler data. The combined effect of increased measurement noise and increased measurement sensitivity may be handled by scaling the nominal one-way data weight by a factor of $\sqrt{2}$. The onboard clock error may be removed or reduced via calibration, which leads to the concept of two-way and pseudo two-way GPS Doppler.

In simulation analyses, the truth onboard clock error is known and can therefore be entirely removed from the one-way GPS Doppler measurements; this data type is referred to as "two-way GPS Doppler". This measurement is now directly analogous to two-way DSN Doppler data, in which the DSN clock errors are not the dominant error source. The two-way GPS Doppler measurements are computed by removing the truth clock signal from the one-way GPS phase data.

$$\phi_{\text{2-way}}(t) = \phi_{\text{1-way}}(t) - c\delta t_r(t) \tag{2}$$

The two-way and one-way phase measurements are denoted as $\phi_{\text{2-way}}$ and $\phi_{\text{1-way}}$, respectively, and δt_r represents the truth receiver clock. The calibrated phase data is then differenced to construct integrated two-way GPS Doppler data as shown in Eq. 1.

In actual flight, however, the true onboard clock error is unknown, and thus cannot be completely calibrated out of the one-way GPS Doppler data. As a proxy, the estimated onboard clock solution δt_r^* can be used to calibrate the one-way GPS phase data, creating pseudo two-way GPS phase measurements ($\phi_{\text{P2-way}}$) in which only the residual clock error remains.

$$\phi_{\text{P2-way}}(t) = \phi_{\text{1-way}}(t) - c\delta t_r^*(t) \tag{3}$$

The estimated clock solution is generated by processing the full GPS data set, yielding orbit and clock solution errors on the order of centimeters and tens of picoseconds, respectively. Analysis of the current DSAC performance has shown that pseudo two-way GPS Doppler data is slightly noisier than two-way GPS Doppler data, as the measurement error at 60 seconds is dominated by the GPS investigation system and is aliased into the clock solution. No additional systematic errors

are introduced through the clock solution calibration. In the absence of true two-way GPS Doppler data, pseudo two-way data may be used as a suitable proxy.

Though in actuality all three data types are physically one-way measurements, comparisons of one-way GPS Doppler, two-way GPS Doppler, and pseudo two-way GPS Doppler provide insight into the navigation performance were true two-way tracking data possible. Note that this work uses GPS Doppler data only; simulation studies have shown that including pseudo-range does not significantly enhance the navigation solution.

Simulated Tracking Schedule

In its current configuration and orientation, at any given time an average of approximately 12 GPS satellites will be visible to the OTB GPS receiver. This dense tracking coverage will be downselected to better represent the more limited DSN tracking of deep space missions. Due to the longitudinal spacing of the DSN complexes, at least one station can track a spacecraft at any given time. Although two ground stations may have simultaneous geometric visibility, onboard hardware limitations constrain two-way tracking to at most one signal at any given time. Conversely, a one-way downlink configuration has no such limitation and the signal could be received simultaneously at two ground stations. To mimic the DSN tracking coverage, the GPS tracking data is downselected to a constellation of 3 co-planar GPS satellites; PRNs 3, 17, and 29 have been selected for this analysis. During the simulation time, PRNs 3, 17, and 29 are distributed approximately evenly throughout their orbital plane. Tracking data is then cut from each of the PRNs to represent the DSN tracking schedule shown in Figure 3 (top). This continuous tracking schedule contains coverage overlaps that may be exploited in a one-way tracking paradigm. The discontinuous two-way tracking schedule (Figure 3, bottom) does not contain any coverage overlaps, as simultaneous two-way radiometric tracking is not realizable. Additionally, 8-hour tracking gaps are inserted to represent periods during which the DSN is committed to tracking other spacecraft. The 8-hour tracking gaps were selected based on actual DSN tracking of MRO, Odyssey, and MAVEN.

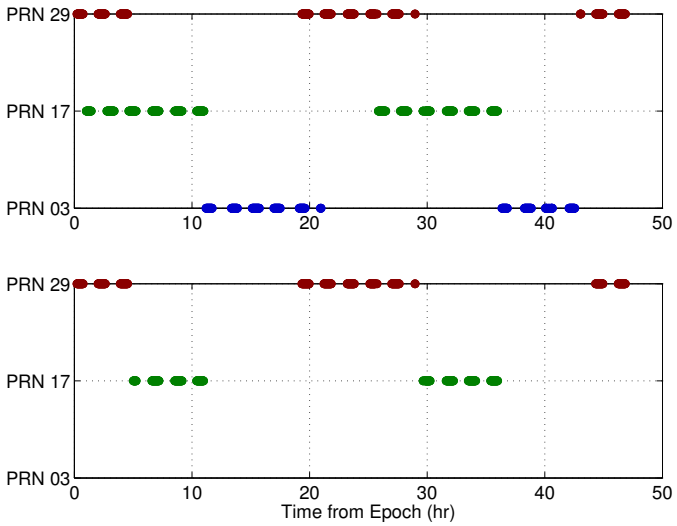

Figure 3. Continuous one-way (top) and discontinuous two-way (bottom) OTB tracking schedules.

High-Fidelity Filter Configuration and Performance

GPS phase and pseudo-range data has been simulated in accordance with the nominal high-fidelity models and expected on-orbit errors, and a clock solution has been estimated (see Reference 3 for further details regarding DSAC precise clock estimation). The filter nominal trajectory is propagated from a perturbed set of initial conditions and the nominal high-fidelity (error-free) models. The filter nominal clock is defined as either the truth clock (two-way Doppler), the solution clock (pseudo two-way Doppler), or a perfect clock (one-way Doppler). Two days of 60-second Doppler measurements from the downselected GPS constellation are constructed in accordance with the one-way (continuous) and two-way (discontinuous) tracking schedules shown in Figure 3. The one-way data uncertainty is defined as 2 cm in phase space ($\approx$ 0.004 Hz) to account for the summation measurement noise; in order to account for the increased measurement sensitivity of true two-way radiometric data, the two-way and pseudo two-way GPS Doppler data weight is defined as $2\sqrt{2}$ cm.

An upper-diagonal sequential Kalman filter/smoother process replicates the high-fidelity MRO operational navigation performed on the ground (Table 2). During MRO operations, the Mars J_{12} and J_{13} zonal gravity terms are recovered due to MRO's orbital sensitivity to these parameters; analogously, as the OTB spacecraft will complete approximately 14.52 orbits in one day, the J_{14} and J_{15} zonal gravity terms are estimated. The filter also estimates ECRV stochastic drag and solar pressure parameters optimally tuned to the expected levels . The filter includes only one accommodation for the one-way data processing, which is to add a clock drift estimate whenever there is a GPS satellite hand-off. This is necessary because of small frequency offsets that would exist between transmitting and receiving hardware. However, this additional estimated stochastic parameter has no substantial impact on the resulting orbit determination solution or associated uncertainty; hence, filtering the one-way DSAC tracking data is essentially the same as filtering traditional two-way tracking data.

Table 2. High-Fidelity Navigation Analog Experiment Filter Configuration

Estimated Parameter	Parameter Type	Uncertainty Model
Position (EME2000)	Dynamic	σ = 1 km
Velocity (EME2000)	Dynamic	σ = 0.23 cm/sec
Gravity / Earth / J_{14}	Bias	σ = 1e-9
Gravity / Earth / J_{15}	Bias	σ = 1e-9
Solar pressure scale factor	Stochastic	ECRV σ = 0.1, τ = 1/2 x orbital period Batch duration = 60 sec
Atmospheric drag coefficient	Stochastic	ECRV σ = 0.1, τ = 30 sec Batch duration = 60 sec
Clock drift (one-way GPS Doppler only)	Stochastic	White noise σ = 1e-9 Estimated at GPS satellite hand-offs

The simulation results presented in Reference 3 demonstrate that the OTB orbit can be recovered to sub-meter level when utilizing either the continuous or discontinuous downselected GPS tracking schedule. The introduction of 8-hour tracking gaps inflates the orbit uncertainty by only 25 cm during the coverage gaps. There is essentially no differentiation between the solutions resulting

from one-way, two-way, or pseudo-two way GPS Doppler processing, indicating that the clock is not the dominant error source and that the one-way performance is on par with the two-way performance. During tracking, the two-way uncertainty bounds are slightly smaller than the one-way uncertainty bounds due to the increased data weight compensating for increased measurement sensitivity. Furthermore, the pseudo two-way GPS Doppler is shown to be a suitable surrogate for true two-way GPS Doppler data. During operations, the precise orbit determination derived from all available GPS tracking data is expected to yield orbit errors < 10 cm. These high precision results can be used as truth to unambiguously evaluate the performance of the deep space analog orbit determination experiment.

ONBOARD NAVIGATION ANALOG EXPERIMENT

The nominal DSAC navigation analog experiment satisfies the mission requirement with ample margin, and is reflective of the performance of traditional ground-based orbit determination operations. During such ground operations, computational efficiency and data storage are effectively not limiting factors, and as such high-fidelity dynamic and measurement models and optimally-tuned filter configurations may be used. Additionally, information such as spacecraft attitude telemetry, small forces, and media calibrations are available for post-processing orbit reconstruction.

In contrast, the computational efficiency and data storage available to an onboard filter will be limited by the spacecraft computer architecture, and the nominal models and filter configuration must be simplified accordingly. Piping attitude telemetry and small force telemetry to the filter complicates the data flow, and would require onboard filtering of the raw data. While general media models may be available onboard, the empirically-determined media calibrations produced by the DSN will not be available in real-time. This work focuses on simplifications to the filter configuration and nominal dynamic models, and assesses the degradation of orbit determination solutions given such simplifications.

Filter Simplications

The optimally-tuned filter presented in Table 2 may be simplified by estimating stochastic accelerations to account for all errors instead of the tuned atmospheric drag, solar radiation pressure, and clock stochastic processes. The stochastic accelerations are estimated in the spacecraft-fixed Radial, Tangential, and Normal (RTN) frame. The structure and weighting of the acceleration stochastic processes are determined through evaluation of the Allan Deviations of the modeling errors. The simplified filter configuration is summarized in Table 3.

The overlapping Allan Deviations of the nominal high-fidelity model RTN acceleration errors, comprised of only the acceleration differences introduced by the errors shown in Table 1, are shown in Figure 4. The Allan Deviations, $\sigma_y(\tau)$, reveal that while the acceleration errors in all three directional components are primarily white, the radial and tangential components also exhibit underlying ECRV behavior. To compensate for the dominant noise structure present in each acceleration component, the filter stochastic acceleration parameters are tuned as white noise processes. The tuned process noise uncertainties (σ_R, σ_T, and σ_N) are shown in Figure 4; these values are determined by mapping the long term Allan Deviation to the data interval (60 seconds), assuming white acceleration noise. The 60-second Allan Deviation is then mapped to the standard variance σ as[6]

$$\sigma^2 = \frac{\tau^2 \sigma_y^2(\tau)}{3} \tag{4}$$

Table 3. Onboard Navigation Analog Experiment Filter Configuration

Estimated Parameter	Parameter Type	Uncertainty Model
Position (EME2000)	Dynamic	σ = 1 km
Velocity (EME2000)	Dynamic	σ = 0.23 cm/sec
Gravity / Earth / J_{14}	Bias	σ = 1e-9
Gravity / Earth / J_{15}	Bias	σ = 1e-9
Radial Acceleration	Stochastic	Determined from Allan Deviation Batch duration = 60 sec
Tangential Acceleration	Stochastic	Determined from Allan Deviation Batch duration = 60 sec
Normal Acceleration	Stochastic	Determined from Allan Deviation Batch duration = 60 sec

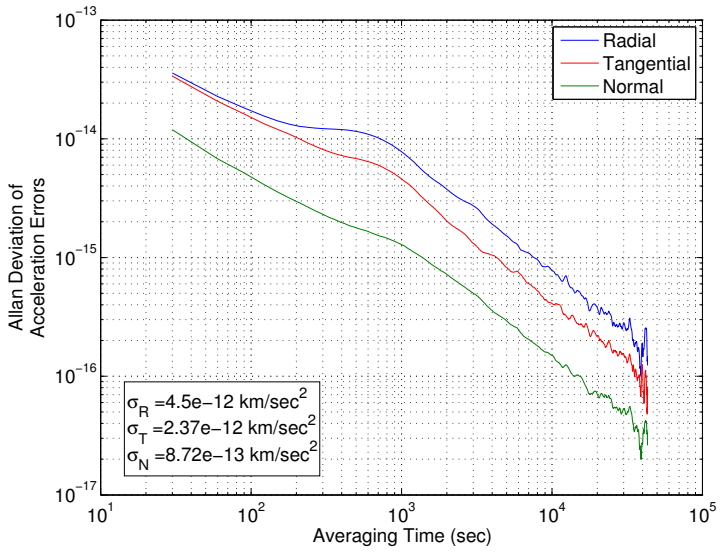

Figure 4. Allan Deviation of high-fidelity model acceleration errors.

The tuned simplified filter, consisting of a linearized Kalman filter and no smoother, was then utilized to process simulated measurements generated with the high-fidelity nominal models and the error sources summarized in Table 1. The simplified and optimally-tuned filters demonstrate similar orbit reconstruction performance. The orbit position errors and 3σ uncertainty envelopes of the simplified filter solution when processing one-way GPS Doppler data are shown in Figure 5. The steady-state position error RMS is $\approx$ 17 cm, and the maximum eigenvalue of the covariance matrix is $\approx$ 65 cm (3σ). This result is comparable with the high-fidelity filter results presented in Reference 3.

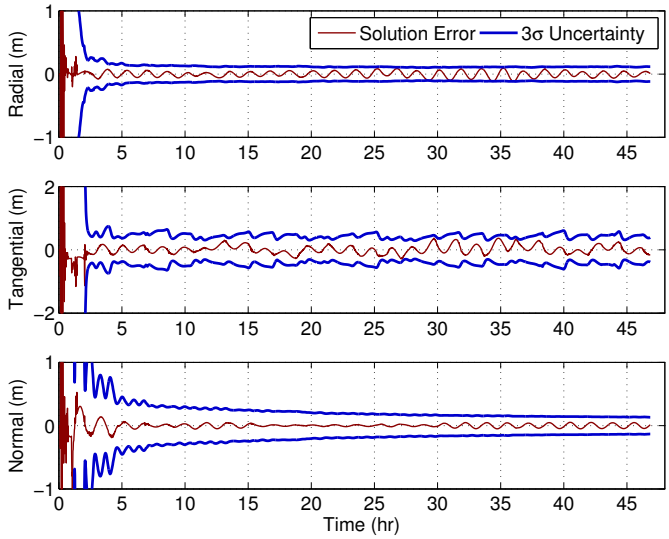

Figure 5. Orbit position errors and 3σ uncertainty bounds for simplified filter configuration (one-way GPS Doppler).

Dynamic Model Simplications

Reductions in the fidelity of the dynamic models are next investigated as a means of lowering the computational requirements of an onboard filter. The low-fidelity dynamic model simplifications include a truncated gravity field, approximations of the spacecraft surface material properties, and approximations of the atmospheric density. Additionally, the necessity of real-time attitude telemetry filtering is removed by reducing the OTB spacecraft from the 8-plate model to an attitude-independent sphere.

Spherical Harmonic Gravity Model The high-fidelity Earth gravitational model consists of the EGM-96 360x360 static gravity potential, with coefficients defined in a 5.1 MB file. Analysis of the acceleration errors introduced by truncating the gravity field shows that the errors are predominantly white noise, with ECRV behavior at low averaging times when the field size is truncated below 45x45. By truncating the filter nominal gravity field and size and tuning the stochastic RTN accelerations via the acceleration error Allan Deviations, an assessment of the impact of gravity field truncation on filter performance was performed. Figure 6 presents the filter run time and the orbit position error root mean square (RMS) for truncated gravity fields. While run time increases monotonically with field size, solution improvement plateaus after degree and order 90. A gravity field size of 45x45 was selected for this work to be commensurate with the meter-level orbit accuracies typical for MRO orbit reconstruction, while gaining a 30% improvement in run time. Truncating the gravity field to 45x45 also reduces the coefficient file size from 5.1 MB to 86 KB.

Spacecraft Surface Reflectivity The high-fidelity spacecraft shape model consists of 8 flat plates with semi-empirically determined specular and diffuse reflectivity parameters. As shown in Figure 1, the OTB spacecraft bus has solar panels on nearly every surface; only the -Y and +Z bus surfaces do not have solar panels and are not highly absorptive. In order to reduce the multi-plate spacecraft model to a sphere, representative diffuse reflectivity surface material properties must be determined. A weighted average reflectivity coefficient, $\bar{\nu}_d(t)$, was computed by assessing the sun-facing area of the 8-plate model given the nominal attitude profile.

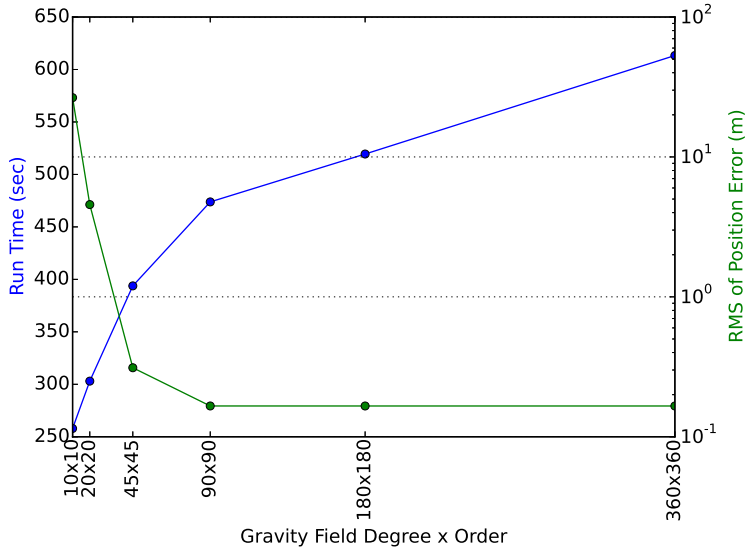

Figure 6. Impact of spherical harmonic gravity model size on filter performance.

$$\bar{\nu}_d(t) = \sum_{i=1}^{8} \frac{a_{\odot,i}(t)}{A_{\odot}(t)} \nu_{d,i} \tag{5}$$

In Equation 5, $a_{\odot,i}(t)$ denotes the sun-facing area of plate i at epoch t, $A_{\odot}(t)$ denotes the the total sun-facing area at epoch t, and $\nu_{d,i}$ is the diffuse reflectivity factor of plate i. Likewise, a weighted average degradation factor, $\bar{\kappa}_d(t)$, was computed as shown in Equation 6.

$$\bar{\kappa}_d(t) = \sum_{i=1}^{8} \frac{a_{\odot,i}(t)}{A_{\odot}(t)} \kappa_{d,i} \tag{6}$$

The weighted average diffuse reflectivity coefficient over six orbits is shown in Figure 7. Earth shadowing and self-shadowing effects are not taken into account (self-shadowing is also not included in the high-fidelity models). The minimum values reflect the high absorptivity of the solar arrays as the sun vector is predominantly in the zenith direction. The angle between the Earth-Sun position vector and the orbital plane (β) is approximately 20°. The time average of the weighted average diffuse reflectivity coefficient is 0.1459. The diffuse reflectivity degradation factor for each of the 8 plates is 1.0, hence the average degradation factor is simply 1.0. As discussed in Reference 2, a spherical spacecraft shape model can not capture the spectral reflectivity of a flat plate model, and hence the solar pressure component in the plane of a flat plate cannot be accounted for.

Atmospheric Density High-fidelty atmospheric density is via the Drag Temperature Model (DTM) developed and maintained by the Centre National d'Etudes Spatiales (CNES). DTM is a semi-analytic model based on temperature, density, and thermosphere composition data collected by satellites at a variety of altitudes.[7] This work utilizes the DTM-2012 model update developed by the CNES Advanced Thermosphere Model for Orbit Prediction (ATMOP) project. The DTM-2012

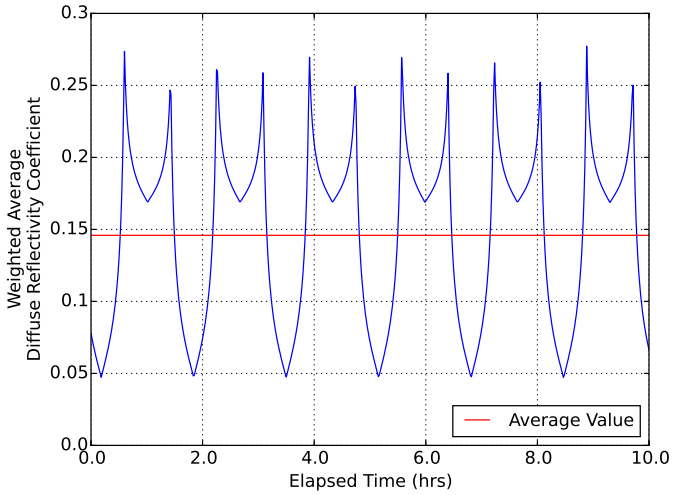

Figure 7. Weighted average diffuse reflectivity coefficient computed from multi-plate spacecraft shape model.

model computes the total atmospheric density based on solar flux, geomagnetic activity, thermosphere constituents, satellite altitude, latitude, and local solar time.[8]

A simplified atmospheric density model was developed by performing polynomial fits to subsets of the DTM-2012 densities with true local solar time (TLST, θ) as the independent variable. The data subsets separate the DTM-2012 densities into sunlight and shadow, with the shadow component broken down into small TLST (0 to 5 hours) and large TLST (20 to 24 hours) to mitigate numerical instabilities in the partial derivative computations. In practice, when necessary updated DTM-2012 densities could be computed on the ground and updated polynomials uploaded to the spacecraft. Figure 8 shows the DTM-2012 densities and the polynomials model for the simulation time period; the maximum error in the polynomials model is $\approx 20\%$. The polynomials model, referred to as the PolyDen model, is comprised of the following, where θ is in radians:

$$f(\theta) = \begin{cases} f_1(\theta), & \text{if } \theta \in [5 \text{ hr}, 20 \text{ hr}] \\ f_2(\theta), & \text{if } \theta \in [0 \text{ hr}, 5 \text{ hr}) \\ f_3(\theta), & \text{if } \theta \in (20 \text{ hr}, 24 \text{ hr}) \end{cases} \tag{7}$$

$$f_1(\theta) = 7.29\text{e-}10(\theta^5) - 4.33\text{e-}8(\theta^4) + 9.41\text{e-}7(\theta^3) - 9.30\text{e-}6(\theta^2) + 4.34\text{e-}5(\theta) - 6.83\text{e-}5 \tag{8}$$

$$f_2(\theta) = 1.47\text{e-}8(\theta^3) + 1.32\text{e-}8(\theta^2) - 4.58\text{e-}7(\theta) + 9.34\text{e-}6 \tag{9}$$

$$f_3(\theta) = -8.96\text{e-}8(\theta^3) + 6.19\text{e-}6(\theta^2) - 1.43\text{e-}4(\theta) + 1.11\text{e-}3 \tag{10}$$

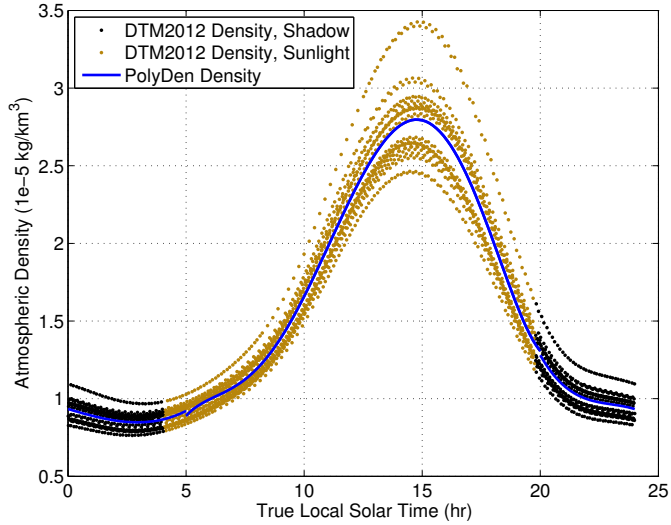

Figure 8. DTM-2012 and PolyDen atmospheric density as a function of true local solar time.

Spacecraft Shape The spherical OTB representation must be sized to appropriately account for the solar radiation pressure and atmospheric drag accelerations of the multi-plate shape model. The solar pressure acceleration, $\vec{a}_{SRP}(t)$, for a spherical spacecraft is modeled as:

$$\vec{a}_{SRP}(t) = -\frac{Sf(t)C}{mR_{\odot}(t)^2}\left\{\pi r^2\left(1+\frac{4}{3}\kappa_d\nu_d\right)\right\}\hat{u}_{\odot}(t) \tag{11}$$

in which S is the solar pressure scale factor (nominally 1), $f(t)$ is the shadowing scale factor (nominally 1 when the spacecraft is in sunlight and 0 when in shadow), C is the solar flux at 1 AU, m is the spacecraft mass, $R_{\odot}(t)$ is the distance from the spacecraft to the sun, r is the spherical pacecraft radius, and $\hat{u}_{\odot}(t)$ is the spacecraft to sun directional unit vector.

The effective solar pressure spacecraft radius is computed by evaluating Equation 11 with the high-fidelity solar pressure acceleration and the weighted average reflectivity and degradation parameters $\bar{\nu}_d$ and $\bar{\kappa}_d$.

The computed solar pressure radius is shown in Figure 9; the mean radius value is 0.74 m.

Likewise, the high-fidelity drag acceleration is used to solve for an effective drag spacecraft radius. The drag acceleration, $\vec{a}_{Drag}(t)$, is given by

$$\vec{a}_{Drag}(t) = \frac{-\rho(t)C_D\pi r^2 v_B(t)^2}{2m}\hat{v}_B(t) \tag{12}$$

in which $\rho(t)$ is the atmospheric density, C_D is the drag coefficient (nominally 2.5), and $\vec{v}_B(t)$ is the body-fixed velocity vector. The effective drag radius is computed by evaluating Equation 12 with the high-fidelity drag acceleration and the PolyDen density model. The drag radius and its mean value (0.38 m) are also shown in Figure 9. The mean drag radius is nearly half the size of the mean solar pressure radius. Due to this size disparity, independent drag and solar pressure spherical spacecraft models are defined for the low-fidelity dynamic modeling.

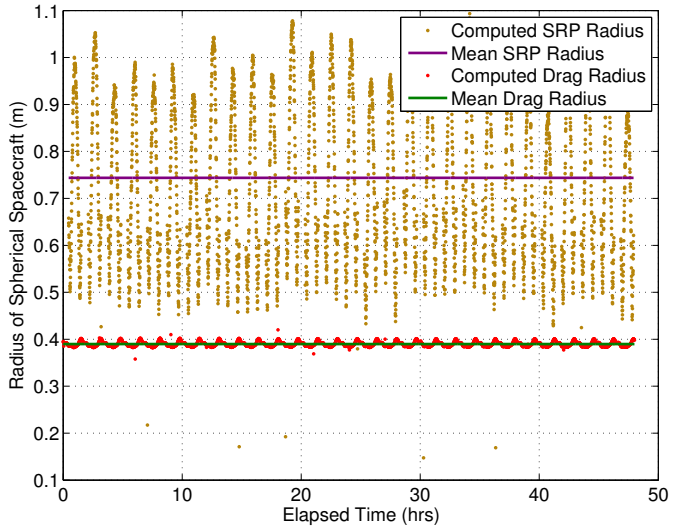

Figure 9. Effective solar pressure and drag spacecraft radii.

Low-Fidelity Model Acceleration Errors The simplified dynamic models now represent a system that is reduced in computational complexity and run time, and free of attitude knowledge requirements. The low-fidelity dynamic model includes a 45x45 EGM-96 gravity field, Newtonian luni-solar gravity, solar pressure modeled with the weighted average reflectivity parameters and the solar pressure spherical spacecraft model, atmospheric drag modeled with the PolyDen density model and the drag spherical spacecraft model, and no Earth albedo and thermal emissivity pressure. (The effect of Earth albedo and thermal emissivity pressure is orders of magnitude smaller than the dominant spacecraft dynamics, and as such is simply neglected in the low-fidelty model.) The Allan Deviations of the acceleration differences between the low-fidelity and high-fidelity models are shown in Figure 10. The errors of the low-fidelity model are dominated by the 45x45 gravity field. All other errors are at least an order of magnitude smaller. The drag errors and albedo pressure errors are commensurate with the nominal acceleration errors of the high-fidelity model (Table 1).

The simplified filter stochastic accelerations are tuned according to the Allan Deviations of the low-fidelity model acceleration errors expressed in the RTN frame, shown in Figure 11. The acceleration errors are predominantly white noise, with 60-second noise strengths as shown in the figure. The filter's stochastic accelerations are tuned to reflect the information given by the Allan Deviations.

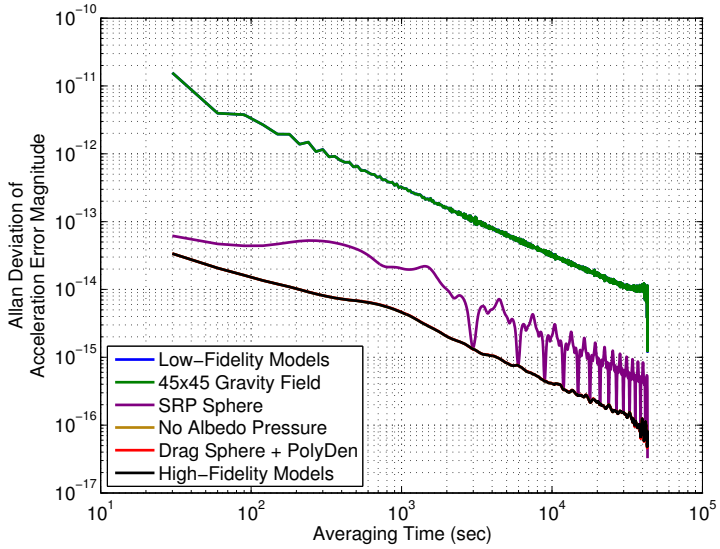

Figure 10. Allan Deviation of acceleration error magnitude for various modeling simplifications.

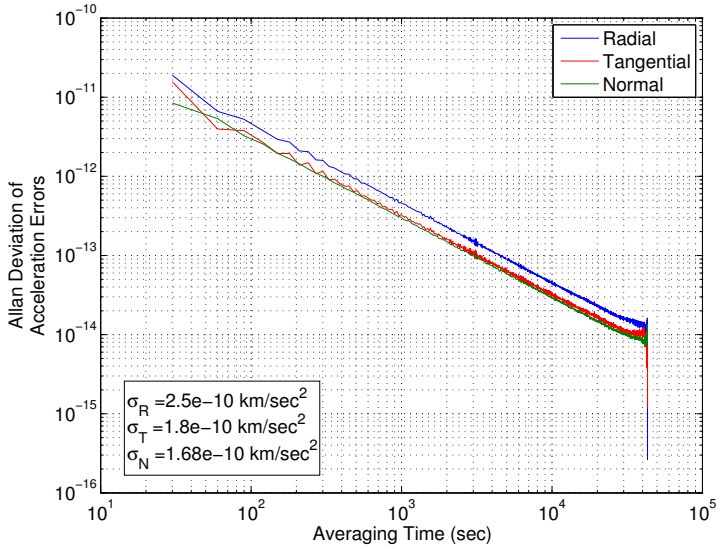

Figure 11. Allan Deviation of low-fidelity model acceleration errors.

Filter Performance

The linear Kalman filter orbit reconstruction results given the low-fidelity dynamic models, the simplified filter configuration tuned to account for the low-fidelity dynamic model errors, and one-way GPS Doppler tracking data are shown in Figure 12. The filter solution uncertainty is representative of the orbit reconstruction errors, indicating that the tuned stochastic accelerations are sufficient to capture the dynamic modeling errors. Over periods when the GPS signal is occulted by the Earth, the tangential uncertainty inflates to ≈ 5 m (3σ), driven by the accumulation of the stochastic accelerations process noise over the tracking gaps. As the entire DSAC clock error is manifested in the one-way GPS Doppler measurement and is not accounted for by the filter design and tuning, it can

be concluded that the low-fidelity orbit reconstruction solution is not significantly impacted by the onboard clock errors.

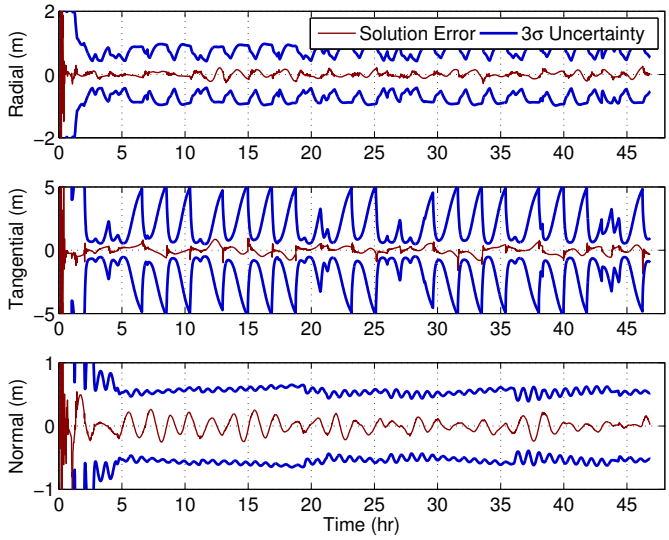

Figure 12. Orbit position errors and 3σ uncertainty bounds for low-fidelity models and simplified filter configuration (one-way GPS Doppler).

The low-fidelity linear Kalman filter is next utilized to process two-way and pseudo two-way GPS Doppler data, following the discontinuous tracking schedule presented in Figure 3. The orbit reconstruction results, shown in Figure 13, show no discernible difference between the two-way and pseudo two-way solutions, further demonstrating pseudo two-way data's suitability to serve as a proxy to actual two-way data during flight. Over the long tracking gaps, the stochastic accelerations act to inflate the covariance to ≈ 50 m, roughly ten times the high-fidelity smoothed orbit reconstruction performance given two-way DSN Doppler tracking of a Mars orbiter.[9] Though the orbit solution quality is significantly degraded, the low-fidelity results are still consistent with the reconstruction requirements of MRO.

The loss of orbit solution accuracy is compensated by an improvement in filter run time. Figure 14 presents the solution position error TMS (green) against the filter run time (blue) for various simplified models. In general, the solution error and run time are inversely proportional. A slight increase in run time is introduced by executing the PolyDen density model; however, the PolyDen model is the only model not yet scripted in the Monte software's native language, and as such the run time cannot be accurately compared to the other models. Additionally, the run time is greatly reduced by removing the albedo and thermal emissivity pressure models. Though small perturbations, the computational models consist of double integrals of the albedo and thermal emissivity over the spherical cap of the source body (Earth) approximated via series expansions; removing these accelerations is more effective in reducing computation time than truncating the gravity field. Neglecting the albedo and thermal emissivity pressures increases the orbit solution error by < 2 cm; though such an increase may be significant in precise orbit determination, it is $< 10\%$ of the low-fidelity solution error.

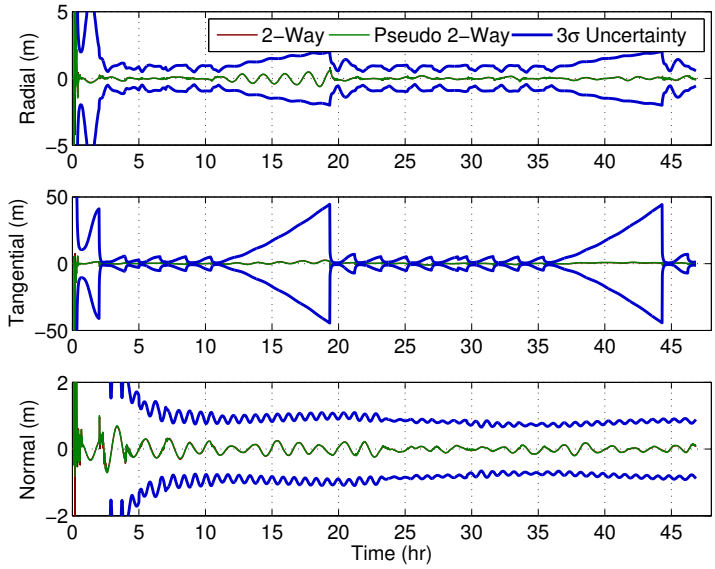

Figure 13. Orbit position errors and 3σ uncertainty bounds for low-fidelity models and simplified filter configuration (two-way and pseudo two-way GPS Doppler data).

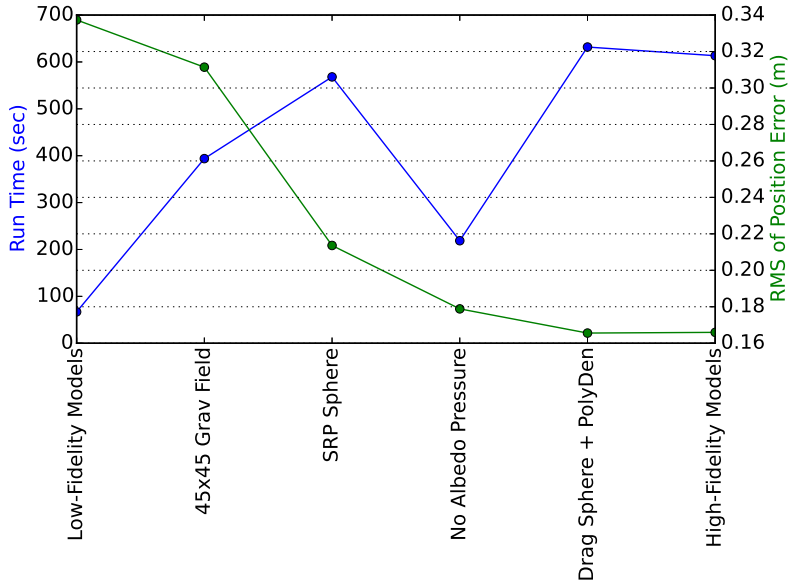

Figure 14. Impact of model simplification on filter performance.

CONCLUSIONS AND FUTURE WORK

Throughout DSAC's yearlong TCM, a planned deep space navigation analog experiment will utilize GPS flight data to demonstrate DSAC's viability as an instrument for ground-based navigation. This work begins to expand upon that baseline deep space analog experiment to demonstrate DSAC's potential for onboard navigation using a one-way DSN uplink. The transition to onboard navigation introduces computational limitations that are not an issue for traditional ground-based

navigation. Several dynamic model and filter configuration simplifications with the potential to increase computational efficiency were investigated. The largest run time improvement stems from truncating the Earth spherical harmonic gravity field to 45x45; this truncation also corresponds to the largest increase of orbit reconstruction errors (15 cm RMS). The low-fidelity dynamic model, including simplifications to the gravity field, atmospheric density, solar pressure, and spacecraft shape model, results in 5 m (3σ) orbit uncertainty when processing continuous one-way GPS Doppler data. Due to the tuned stochastic accelerations, the orbit uncertainty increases to 50 m (3σ) during 8-hour tracking gaps representative of two-way DSN tracking. The one-way, two-way, and pseudo two-way GPS Doppler solution show that if DSAC performs at its anticipated level, the clock errors do not contribute greatly to the orbit solution errors.

This work will be continued to assess the possibility of a constant atmospheric density model; as the acceleration errors are dominated by the reduced gravity field, a constant density may be accurate enough to maintain the solution quality presented herein. Simplifications to the luni-solar gravitational acceleration models will be analyzed, potentially by limited the accuracy of the on-board luni-solar ephemeris information. Furthermore, the robustness of the filter to initial condition error and the practicality of utilizing a linearized Kalman filter will be investigated.

ACKNOWLEDGMENTS

This research was carried out at the Jet Propulsion Laboratory, California Institute of Technology, under a contract with the National Aeronautics and Space Administration.

REFERENCES

[1] N. Hinkley, J. Sherman, N. B. Phillips, M. Schioppo, N. Lemke, K. Beloy, M. Pizzocaro, C. Oats, and A. Ludlow, "An Atomic Clock with 10-18 Instability," *Science*, Vol. 341, September 2013, pp. 1215–1218.

[2] T. A. Ely, J. Veldman, and J. Seubert, "Preliminary Investigtaion of On-Board Orbit Determination Using Deep Space Atomic Clock Based Radio Tracking," *AAS/AIAA Space Flight Mechanics Meeting*, Napa, CA, 2016.

[3] T. A. Ely, D. Murphy, J. Seubert, J. Bell, and D. Kuang, "Expected Performance of the Deep Space Atomic Clock Mission," *AAS/AIAA Space Flight Mechanics Meeting*, Santa Fe, NM, 2014.

[4] J. D. Prestage and G. L. Weaver, "Atomic Clocks and Oscillators for Deep-Space Navigation and Radio Science," *Proceedings of the IEEE*, Vol. 95, November 2007, pp. 2235–2247.

[5] F. G. Lemoine, S. C. Kenyon, J. K. Factor, R. Trimmer, N. K. Pavlis, D. S. Chinn, C. M. Cox, S. M. Klosko, S. B. Luthcke, M. H. Torrence, Y. M. Wang, R. G. Williamson, E. C. Pavlis, R. H. Rapp, and T. R. Olson, "The Development of the Joint NASA GSFC and NIMA Geopotential Model EGM96," tech. rep., NASA Goddard Space Flight Center, Greenbelt, MD, July 1998.

[6] W. J. Riley, "Handbook of Frequency Stability Analysis," tech. rep., National Institute of Standards and Technology, Boulder, CO, 2008.

[7] F. Barlier, C. Berger, J. Falin, G. Kockarts, and G. Thuillier, "A Thermospheric Model Based on Satellite Drag Data," *Annals of Geophysics*, Vol. 34, 1978, pp. 9–24.

[8] S. Bruinsma, N. Sanchez-Ortiz, E. Olmedo, and N. Guijarro, "Evaluation of the DTM-2009 Thermosphere Model for Benchmarking Purposes," *Journal of Space Weather and Space Climate*, Vol. 2, June 2012, pp. 1–14.

[9] T. Ely and J. Seubert, "Advancing Navigation, Timing, and Science with the Deep-Space Atomic Clock," *Space Operations: Innovations, Inventions, and Discoveries* (T. C. Lieuwen, ed.), Vol. 249, pp. 105–137, American Institute of Aeronautics and Astronautics, Inc., 2015.